GCAGS JOURNAL
A Publication of the Gulf Coast Association of Geological Societies
www.gcags.org

Touching-Vug Pore System, Lake Medina Road Cut, Medina County, Texas

F. Jerry Lucia

Bureau of Economic Geology, Jackson School of Geosciences, University of Texas at Austin, University Station, Box X, Austin, Texas 78713–8924, U.S.A.

ABSTRACT

Carbonate pore space has been grouped into matrix and touching-vug pores in order to facilitate merging petrophysical properties and geologic descriptions. Reasonable approaches to merging matrix petrophysics with geology have been developed, but understanding flow in touching vugs and its relationship to geology remains elusive. The road cut through Cretaceous strata near Lake Medina, Medina County, Texas, provides an opportunity to examine the touching-vug problem. The road cut contains a small cave, mostly filled with sediment, numerous fractures and small faults, and vugs of various types and sizes. The cave is associated with a fault with 3 ft (1 m) of offset. Solution-enlarged fractures and bedding-plane dissolution are found associated with the cave. The outcrop contains dolomite and anhydrite that have been calcitized and anhydrite nodules that have been dissolved to form small vugs.

Of primary interest is the dissolution of fractures to form large vugs that are not associated with the cave. These large vugs are located in the beds that have the highest matrix permeability on the outcrop. The permeable beds are described as grain-dominated packstones, whereas other beds are low-permeability, mud-dominated fabrics. Flow modeling by other workers demonstrated that the highest flow rate of groundwater is along the fault and the second highest flow rate is along fractures that intersect the permeable beds. This observation suggests that the distribution of large vugs in a touching-vug pore system is controlled in part by the intersection of permeable fractures and the high-permeability beds. Adding a matrix permeability model to a fracture model may improve predicting the distribution of vuggy pore space in a touching-vug reservoir.

INTRODUCTION

Characterizing carbonate pore systems is an important aspect of building a reservoir model to predict reservoir performance. Carbonate pore systems have been grouped into interparticle pores, separate-vug pores, and touching-vug pores by Lucia (1995a) based on fabric and porosity-permeability considerations. Whereas reasonable approaches to characterize the petrophysical properties of interparticle and separate-vug pores have been developed, characterizing the flow properties of touching-vug pore systems remains elusive. Touching vugs include fracture pores, cavernous pores, and breccia pores. Fractures have been studied in detail as related to structural history. Cavernous pores and associated collapse breccias have also been studied in detail, specifically in the Ellenberger of West Texas (Loucks, 1999; Lucia, 1995b), but applying this information to a carbonate reservoir is difficult.

The patterns of many caves in carbonates can be shown to be controlled by a preexisting fracture/fault system (Kastning, 1986). Fractures and faults that form in response to an earth stress system provide permeable pathways for groundwater to flow and dissolve or precipitate carbonate. Dissolution produces vugs of various sizes. If the vugs are large enough to be considered caves, they may break down forming collapse breccias and associated fractures (Loucks, 1999). Whereas the dissolution normally occurs within the meteoric zone, collapse can happen at shallow depths or with deep burial.

The purpose of this research is to describe the relationship between fractures, caves, vugs, and especially the impact of stratigraphy on vug formation. The Cretaceous Edwards Aquifer in Central Texas is an excellent example of a touching-vug reservoir and has been studied extensively (Halihan et al., 2000). Understanding the origin and production of this aquifer presents an opportunity to develop methods for creating a useful petrophysical model of a subsurface touching-vug reservoir. This study is focused on a road cut in Cretaceous limestone located on FM 1283 just east of Lake Medina in Medina County, Texas (Fig. 1). The road cut consists of vertical walls on either side of FM 1283 (Fig. 2). The major features observed in the road cut

Manuscript received March 21, 2019; revised manuscript received May 16, 2019; manuscript accepted August 20, 2019.

GCAGS Journal, v. 8 (2019), p. 57–70.
DOI: pending

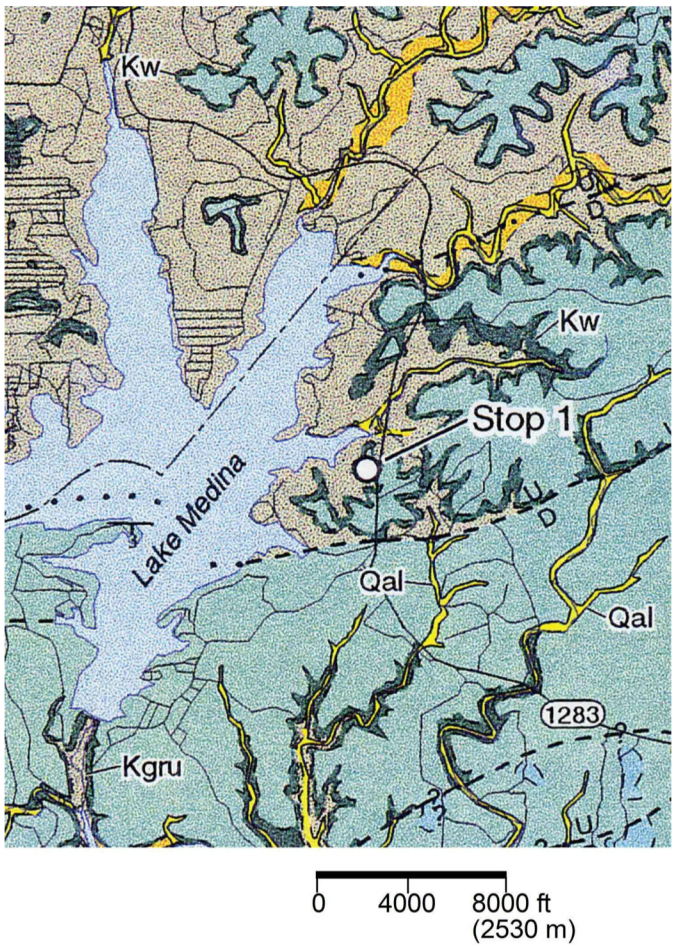

Figure 1. Geologic map showing locations of road cut and major faults. Map colors have been modified. Abstracted from Collins (2000).

are two small caves observed on the west wall and a sediment-filled cave that extends from the bottom to top of the east wall. The road cut also contains vugs of various sizes and shapes along with various fractures and faults. Hovorka et at. (1998) have pointed out that in the Medina outcrop large vugs are preferentially developed at the junction of fractures and dolomitic beds and caves are localized along faults. This study enlarges on that observation.

GEOLOGICAL SETTING

The Cretaceous interval exposed in the Lake Medina road cut is in the lower part of the Edwards Group. Although the contact with the underlying Glen Rose Formation is not well exposed, tracing beds on aerial photographs projects the contact near the northern base of the road cut (Hovorka and Mace, 1997). The transgressive sequence between the Glen Rose and the Edwards, known as the Walnut Formation or the basal nodular member of the Kainer Formation, is present as 21 ft (6.4 m) of intensely burrowed packstones and massive to laminated grainstone. Overlying this unit is an interval of more cyclic and better-bedded algal-foram-mollusk grainstones, grain-dominated packstones, and wackestones reflecting cyclic deposition of the lower Edwards Group. The Edwards Group was buried to a depth of at least 7000 ft (2134 m) before being uplifted during the Miocene and eroded to its present position (Fullmer and Lucia, 2005). The major episode of karst formation in the Edwards Group began after the Miocene uplift and continues today (Veni, 1987).

The outcrop is located within the Balcones Fault Zone, which is composed of a series of echelon normal faults that strike mostly N40–70°E, dip southeastward, and have 100 to 850 ft (30.5 to 259 m) of throw (Collins, 1995). The Medina road cut lies within a 4 mi (6.4 km) wide block bounded by two of these normal faults that strike east-northeast and dip southeastward (Fig. 1).

DESCRIPTION

Stratigraphy and Petrophysics

The interval studied in detail is about 15 ft thick. A measured section is illustrated in Figure 3, and examples of the fabrics are illustrated in Figure 4. Three cycles and one partial cycle are illustrated. Cycle A is composed of a lower burrowed wackestone and an upper 1 ft bed of grain-dominated anhydritic dolograinstone. The lower unit (bed 1) has dolomitized burrows that have been calcitized and limestone with dissolved dolomite crystals. The dolomite and anhydrite of the upper unit (bed 2) have also been calcitized. Cycle B is composed of a 4 ft (4.6 m) bed of fossiliferous wackestone (bed 3), capped by a 1 ft (0.3 m) bed of fossiliferous grain-dominated packstone (bed 4). Cycle C is composed of a 3 ft (1 m) bed of miliolid mud-dominated packstone (bed 5), capped by a 0.5 ft (0.15 m) bed of cemented grain-dominated packstone (bed 6). Cycle D is only partially illustrated and is 2 ft (0.6 m) of mud-dominated fabrics (bed 7), topped by a thin marly limestone This bed is interpreted to be a regressive sequence.

Porosity and permeability of the matrix were measured on 1.5 in (3.8 cm) plugs collected by core drilling the outcrop (Fig. 3, Table 1). The mud-dominated fabrics have porosity values ranging from 5.3 to 19.5% and permeability values ranging from 0.2 to 5.1 md. The lower grain-dominated packstone, bed 2, has 20% porosity and 163 md average permeability. The middle grain-dominated packstone (bed 4) has 23% porosity and 68 md permeability. The upper cemented grain-dominated packstone (bed 6) has 7% porosity and 0.17 md permeability. Additional data are presented in Appendix A.

Fractures and Caves

High-angle fractures are abundant throughout the outcrop. The dominant strike is N45°E with two opposing dips, 64°SE and 69°NW. There may be fractures that are oriented near parallel to the road cut faces, but none have been definitively identified. On the east wall, the fractures strike N40–45°E and dip 65–75°SE and NW. A fault is present that strikes N40°E, dips approximately 70°SE, and has a 3 ft (1 m) offset (Fig. 5). A vertical cave has formed along this fault that extends from the road up to the top of the outcrop and is about 5 ft (1.5 m) wide (Fig. 5). Two conjugate faults that strike N45°E and dip 70° and that have small offsets are present to the south and define a small graben. The cave has been filled with sediment and collapse breccia (Fig. 6A). Some beds adjacent to the cave have been heavily leached to form numerous vugs and solution-enlarged fractures (Fig. 6B).

On the west wall a fault is present that strikes N45°E and dips 60°SE and has a 2 ft (0.6 m) offset (Fig. 7). A graben is formed by a conjugate 2 ft (0.6 m) fault to the south with a N40° E strike and a 65°NW dip. The northern fault has a fault breccia (Fig. 8A). Two small caves are found associated with the northern fault located at road level (Fig. 8B). They are floored with sediment and breccia. The extent of these caves is not known, but they do not extend far into the road cut and it is assumed that they connect with the cave on the east wall. As in the eastern cave, the cave walls are heavily leached and fractures are enlarged by dissolution.

Figure 2. Photograph of Medina road cut looking north.

Vugs

Numerous vugs are found in both the east and west outcrops. Vugs are distinguished from caves by size. Vugs are voids not large enough for a person to crawl into. Several different types of vugs are observed. Simple dissolution nodes are found along some fractures with no discernable reason for their location. These are generally small (Fig. 9A). Large vugs are found where fractures intersect permeable beds (Fig. 10). Solution-enlarged fractures are generally found associated with cave development (Fig. 9B). Solution-enlarged bedding planes are also found associated with cave development. Vugs that appear to be dissolved burrows are associated with the dissolved bedding planes (Fig. 9C). Other vugs that are not connected to fractures are thought to be molds of anhydrite nodules (Fig. 9D). Many vugs contain a flooring of red sediment, indicating that they are connected to a flow system.

Vugs come in a range of sizes. Visually, the largest vug sizes appear to be associated with permeable, grain-dominated packstone beds 2 and 4 (Fig. 10). To test this observation, vug sizes were measured by Daniel Kurtzman using lidar techniques (Kurtzman et al., 2009). The cross-sectional area of 141 vugs that contain sediment ranges from less than 1 in^2 (6.5 cm^2) to about 120 in^2 (774 cm^2) and averages about 20 in^2 (129 cm^2) (Fig. 11). Kurtzman et al. (2007) plotted an average vug size against bed permeability and confirmed that the largest vugs are associated with the most permeable beds, which are grain-dominated packstone beds 2 and 4 (Fig. 12).

Importantly, these vugs are located where fractures intersect permeable beds. Three-dimensional lidar imaging of two vugs in bed 2 shows that they are elongated along the strike direction of the associated fractures (Fig. 13), which confirms the fracture control on the location and geometry of the vugs. Assuming that fractures tend to be permeable flow paths and that dissolution is a function of the volume of flow, the highest flow is along the fractures and into high-permeability beds 2 and 4. The result is that dissolution is concentrated where permeable fractures intersect the most permeable beds. It is interesting to note that on the west wall the two small caves are located where permeable beds 2 and 4 intersect the northern graben fault (Fig. 7), suggesting a genetic relationship between the initiation of cave formation and the intersection of the graben fault and permeable beds 2 and 4.

DISCUSSION

The diagenetic history of this outcrop is very complicated. Cycle 1 was originally dolomitic; bed 1 was a dolomitic wackestone with dolomitized burrows, and bed 2 was a dolomitized grain-dominated packstone. The vertical sequence suggests that bed 2 was the top of a high-frequency depositional cycle and may have been deposited in a tidal-flat environment (see Figure 3). Because no evidence of dolomite is observed above bed 2, the dolomitizing water may have originated as refluxing hypersaline water before bed 3 was deposited.

The beds were buried to a depth of about 7000 ft (2134 m) (Fullmer and Lucia, 2005), resulting in the normal compaction and cementation common to all carbonates. Uplift and meteoric diagenesis produced fracturing, karsting, and calcification of the dolomite and anhydrite (Abbott, 1974). Major dissolution along the norther fault produced caves and collapse breccias. A genetic link between fractures, matrix permeability, and the formation of the largest vugs has been suggested. Flow-simulation experiments conducted by Kurtzman et al. (2007) demonstrated that

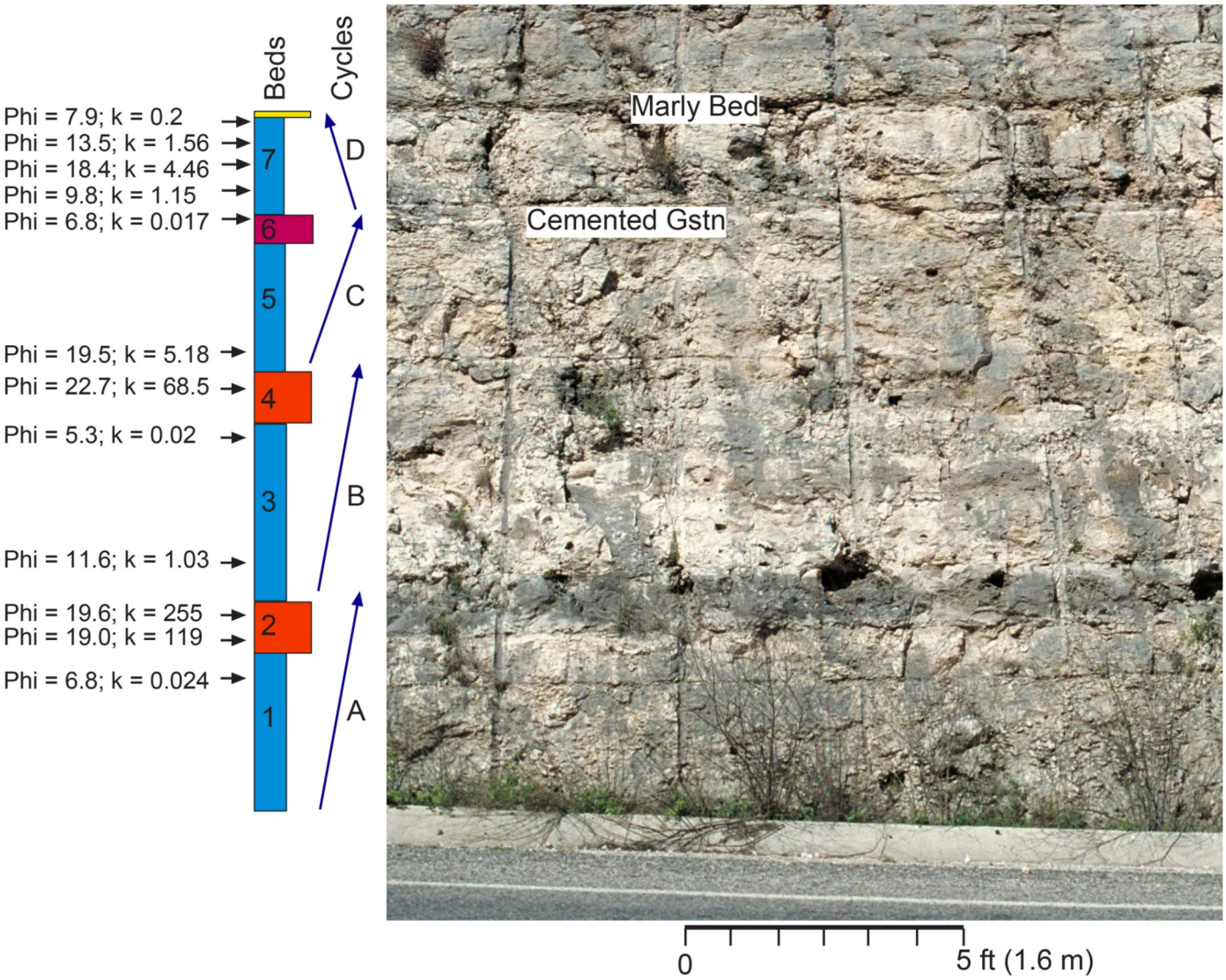

Figure 3. Composite measured section showing beds, cycles, and stratigraphic location of core plugs taken for porosity (%) and permeability measurements (md). The section is show on the east wall although most of the data is from the west wall.

high flow rates are concentrated at the intersections of fractures and permeable beds. It is proposed that the meteoric water flowed down permeable fractures and into permeable beds 2 and 4 at higher rates than down fractures that did not intersect beds 2 and 4. Dissolution occurred preferentially in the permeable beds over dissolution of the fracture walls probably because the surface area of porous beds 2 and 4 is much larger than the surface area of the low-permeability, mud-dominated beds.

Interestingly, the small cave on the west side of the road cut is located where permeable beds 2 and 4 intersect the northern graben fault. The fault breccia associated with this fault suggests that the flow rate along the fault was higher than along other fractures. This high flow rate was magnified in the area where the fault intersects permeable beds 2 and 4, resulting in the initiation of the cave system.

A touching-vug pore system includes not only fracture pore space but also vuggy pore space. Therefore, the distribution of both fracture and vuggy pore space is required to construct a proper flow model. The outcrop model described herein implies that a matrix permeability model as well as a fracture model is required to construct a proper touching-vug permeability model. Linking vug development to permeable beds and fractures present a possible method for distributing large vugs in a touching-vug flow model.

Application to Carbonate Reservoirs

The Pennsylvanian-age Sacroc and Cogdell fields and the Permian-age Hobbs Field found in the Permian Basin of West Texas are known to be fractured and karsted reservoirs having extensive touching-vug pore systems. A number of image logs have been run in these fields that show fractures and large vugs similar in size to the large vugs in the Lake Medina road cut. In addition to image logs, a large number of injection profiles have been run in an attempt to map productive intervals. Many intervals have unusually high injection rates, implying unusually high permeability, and are referred to as "thief zones." Image logs show that these "thief zones" are often associated with intervals with large vugs. However, other intervals are present where the injection rate is high and no vugs or fractures are present in the wellbore (Lucia, 2012). Using this outcrop as a model, these anonymously high injection rates may be due to the presence of a touching-vug pore system composed of permeable fractures and stratigraphically controlled large vugs not present in the well bore.

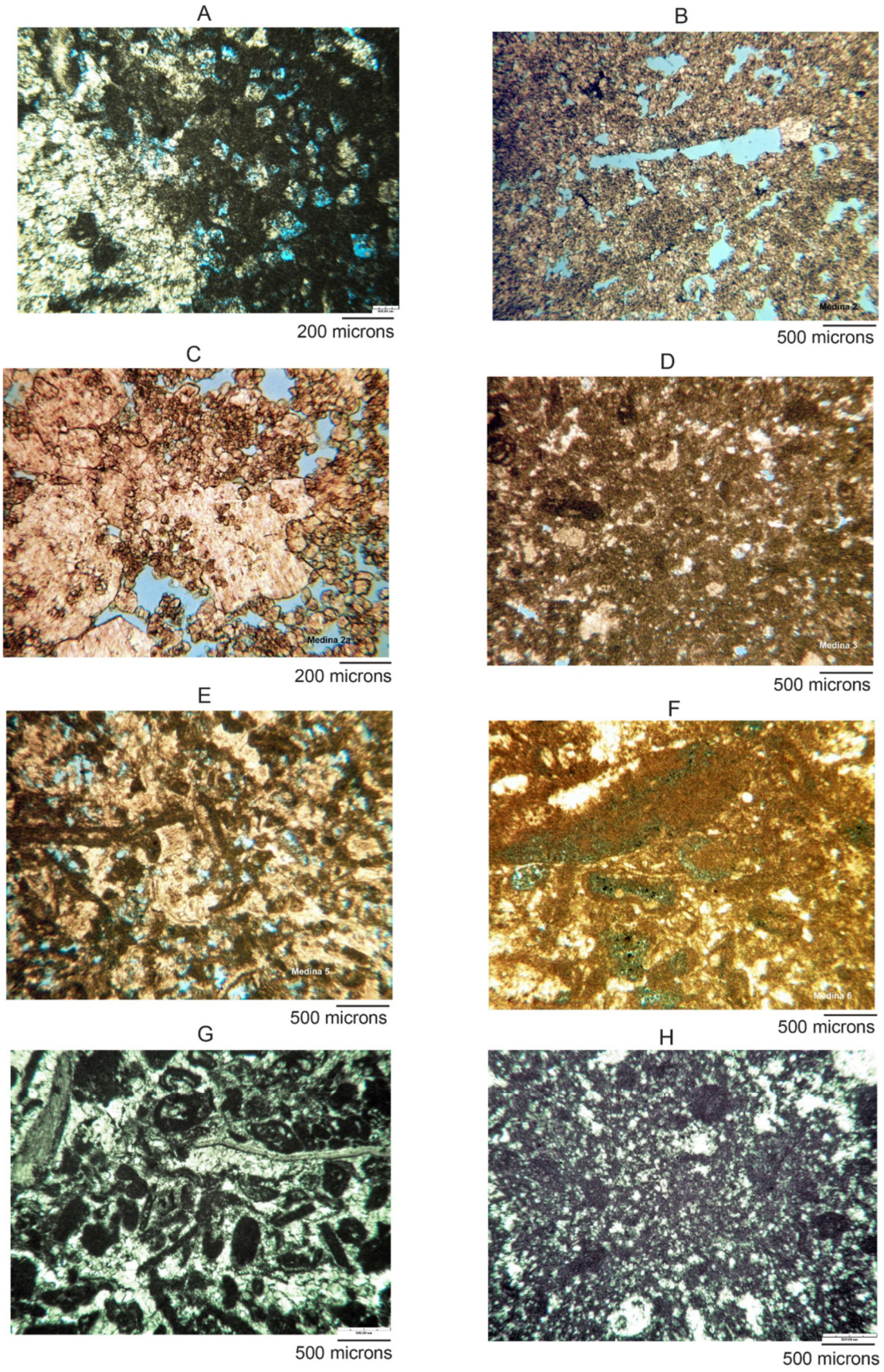

Figure 4. Photomicrographs of stratigraphic beds. (A) Bed 1. Leached dolomite rhombs and calcitized dolostone burrow. (B) Bed 2. Calcitized grain-dominated dolopackstone with fossil molds and intergrain pores. (C) Bed 2. Calcitized grain-dominated dolopackstone with calcitized anhydrite and intercrystal pores. (D) Bed 3. Fossiliferous wackestone. (E) Bed 4. Fossiliferous grain-dominated packstone with intergrain pores. (F) Bed 5. Fossiliferous mud-dominated packstone with intragrain micropores. (G) Bed 6. Grain-dominated packstone with cemented intergrain pore space. (H) Wackestone.

Table 1. Core plug description.

BED NO.	CYCLE NO.	LITHOLOGY	TEXTURE	VISIBLE PORE SPACE				CORE ANALYSIS		NOTES
		Calcite	Rock Fabric	Interpartical Porosity	Separate-Vug Porosity		Touching-Vug Porosity	Por.	Perm.	
		%	Description	%	%	Type	Type	%	md	
1	A	100	Burrowed Wackestone		3	Dissolved Dolomite		6.8	0.24	Calcite and dissolved dolomite crystals, some large mollusks
2	A	100	Calcitized Grain-Dominated Dolopackstone	2	7	Moldic		19.0	119.34	Calcitized dolomite and anhydrite
2	A	100	Calcitized Grain-Dominated Dolopackstone					19.6	255.07	Calcitized dolomite and anhydrite
3	B	100	Fossiliferous Wackestone		tr			11.6	1.03	
3	B	100	Fossiliferous Wackestone					5.3	0.02	
4	B	100	Fossiliferous Grain-Dominated Packstone	7	3	Moldic?		22.7	68.54	
5	C	100	Miliolid Mud-Dominated Packstone					19.5	5.18	
6	C	100	Cemented Grain-Dominated Packstone					6.8	0.17	
7	D	100	Burrowed Wackestone					9.8	1.15	
7	D	100	Wackestone					18.4	4.46	
7	D	100	Peloidal Mud-Dominated Packstone					13.5	1.56	
7	D	100	Peloidal/ Fossiliferous Mud-Dominated Packstone					7.9	0.20	

CONCLUSIONS

The road cut on FM 1283 just east of Lake Medina is an excellent example of how fractures and stratigraphy control the origin and distribution of large vugs and caves. The location of the cave is controlled by a 3 ft (1 m) fault. The location of large vugs is controlled by two high-permeability beds and fracture intersections.

The dissolution was controlled by the volume of water flow. The highest water flow was along the largest graben fault and, initially, in high-permeability beds 2 and 4. This flow produced the caves found in the road cut. Away from the fault, the highest flow was along permeable fractures that intersected high-permeability beds 2 and 4. This flow enlarged the fractures in the vicinity of beds 2 and 4, forming large vugs.

This dissolution model could account for intervals in karsted reservoirs where flow is anomalously high and neither fractures nor vugs are found in the well bore to account for the high flow rate. In addition, it suggests that both a fracture and a matrix permeability model are necessary to model the distribution of vuggy porosity.

ACKNOWLEDGMENTS

This research was funded by the many industrial members of the Carbonate Reservoir Characterization Research Laboratory of the Bureau of Economic Geology, Jackson School of Geosciences, University of Texas at Austin. The author would like to thank his colleagues, Xavier Janson, Chris Zahm, and Robert Loucks, for their assistance with this research. William Rader edited the

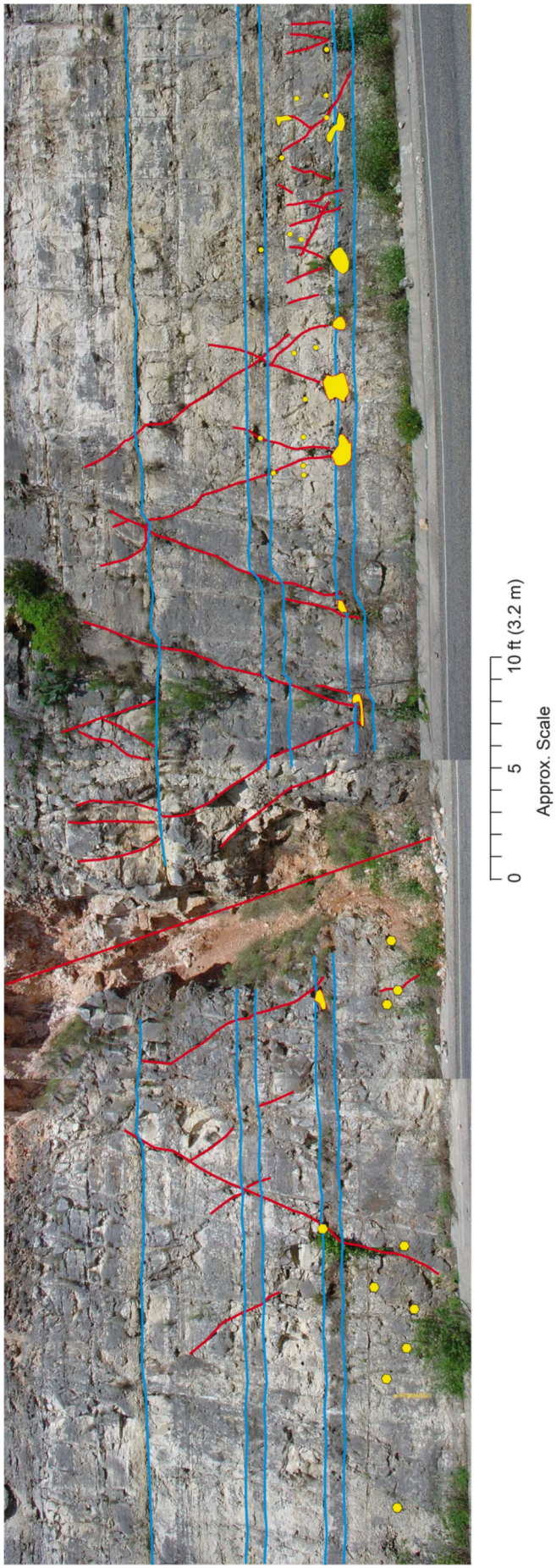

Figure 5. East face of road cut showing vertical cave filled with sediment along a normal fault. Major fractures are marked in red. Beds 2 and 4 and the upper marly bed are marked in blue. Vugs are shown in yellow. Photo is oriented north (left) to south (right).

paper. Comments by technical reviewers J. M. Sharp and S. M. Fullmer were very helpful. Publication authorized by the Director, Bureau of Economic Geology.

REFERENCES CITED

Abbott, P. L., 1974, Calcitization of Edwards Group dolomites in the Balcones Fault Zone aquifer, south-central Texas: Geology, v. 2, p. 359–362.

Collins, E. W., 1995, Structural framework of the Edwards Aquifer, Balcones Fault Zone, Central Texas: Gulf Coast Association of Geological Societies Transactions, v. 45, p. 135–142.

Collins, E. W., 2000, Geologic map of the New Braunfels, Texas, 30 x 60 minute quadrangle: Geologic framework of an urban-growth corridor along the Edwards Aquifer, south-central Texas: Bureau of Economic Geology, Miscellaneous Map 39, Austin, Texas, scale 1:100,000, 28 p. text.

Fullmer, S., and F. J. Lucia, 2005, Burial history of Central Texas Cretaceous carbonates: Gulf Coast Association of Geological Societies Transactions, v. 55, p. 225–232.

Halihan, T., R.E. Mace, and J.M. Sharp, Jr., 2000, Flow in the San Antonio segment of the Edwards aquifer: matrix, fractures, or conduits?, *in* C. M. Wicks and I. D. Sasowsky, eds., Groundwater flow and contaminant transport in carbonate aquifers: AA Balkema, Rotterdam, Netherlands, p. 129–146.

Hovorka, S. D., and R. E. Mace, 1997, Interplay of karst, fractures, and permeability in the Cretaceous Edwards Aquifer: Analogs for fractured carbonate reservoirs: Geological Field Trip, Society of Petroleum Engineers Annual Technical Conference and Exhibition Field Trip Guidebook, published by Bureau of Economic Geology, Austin, Texas, 35 p.

Hovoka, S. D., R. E. Mace, and E. W. Collins, 1998, Permeability structure of the Edwards Aquifer, South Texas—Implications for aquifer management: Bureau of Economic Geology Report of Investigations 250, Austin, Texas, 55 p.

Kastning, E. H., 1986, Cavern development in the New Braunfels area, Central Texas, *in* P. L. Abbott, P. L., and C. M. Woodruff, Jr., 1986, The Balcones Escarpment: University of Texas at Austin, p. 91–100, <www.lib.utexas.edu/geo/balcones_ escarpment/balconesescarpment.html>.

Kurtzman, D., J. A. El Azzi, F. J. Lucia, J. A. Bellian, C. Zahm, and X. Janson, 2009, Improving fractured carbonate-reservoir characterization with remote sensing of beds, fractures, and vugs: Geosphere, v. 5, p. 126–139, <https://doi.org/10.1130/GES00205.1>.

Kurtzman, D., J. W. Jennings, Jr., and F. J. Lucia, 2007, Dissolution vugs in fractured carbonates: A complication? Or perhaps a key for simplifying reservoir characterization: Geophysical Research Letters, v. 34, 6 p., <https://doi.org/10.1029/2007/GL031229>.

Loucks, R. G., 1999, Paleocave carbonate reservoirs: Origins, burial-depth modifications, spatial complexity, and reservoir implications: American Association of Petroleum Geologists Bulletin, v. 83, p. 1795–1834.

Lucia F. J., 2012, RCRL studies of thief zones in Sacroc Field: Report prepared by the Bureau of Economic Geology (Austin, Texas) for Kinder Morgan Company, 22 p.

Lucia, F. J., 1995a, Chapter 14, Lower Paleozoic cavern development, collapse, and dolomitization, Franklin Mountains, El Paso, Texas, *in* D. A. Budd, A. H. Saller, and P. M. Harris, eds., Unconformities and porosity in carbonate strata: American Association of Petroleum Geologists Memoir 63, Tulsa, Oklahoma, p. 279–300.

Lucia, F. J., 1995b, Rock-fabric/petrophysical classification of carbonate pore space for reservoir characterization: American

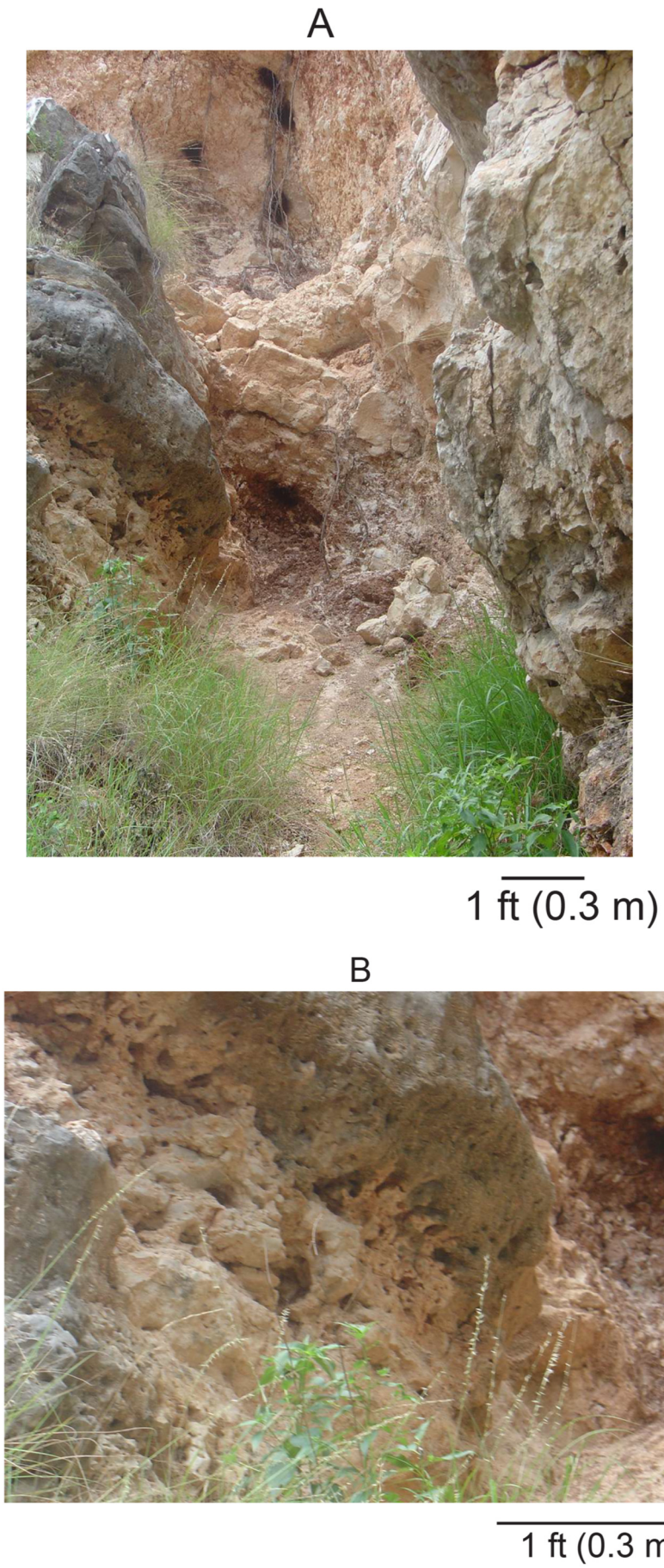

Figure 6. East wall cave. (A) Collapse breccia and sediment infill. (B) Extensive large vugs in the wall of east cave.

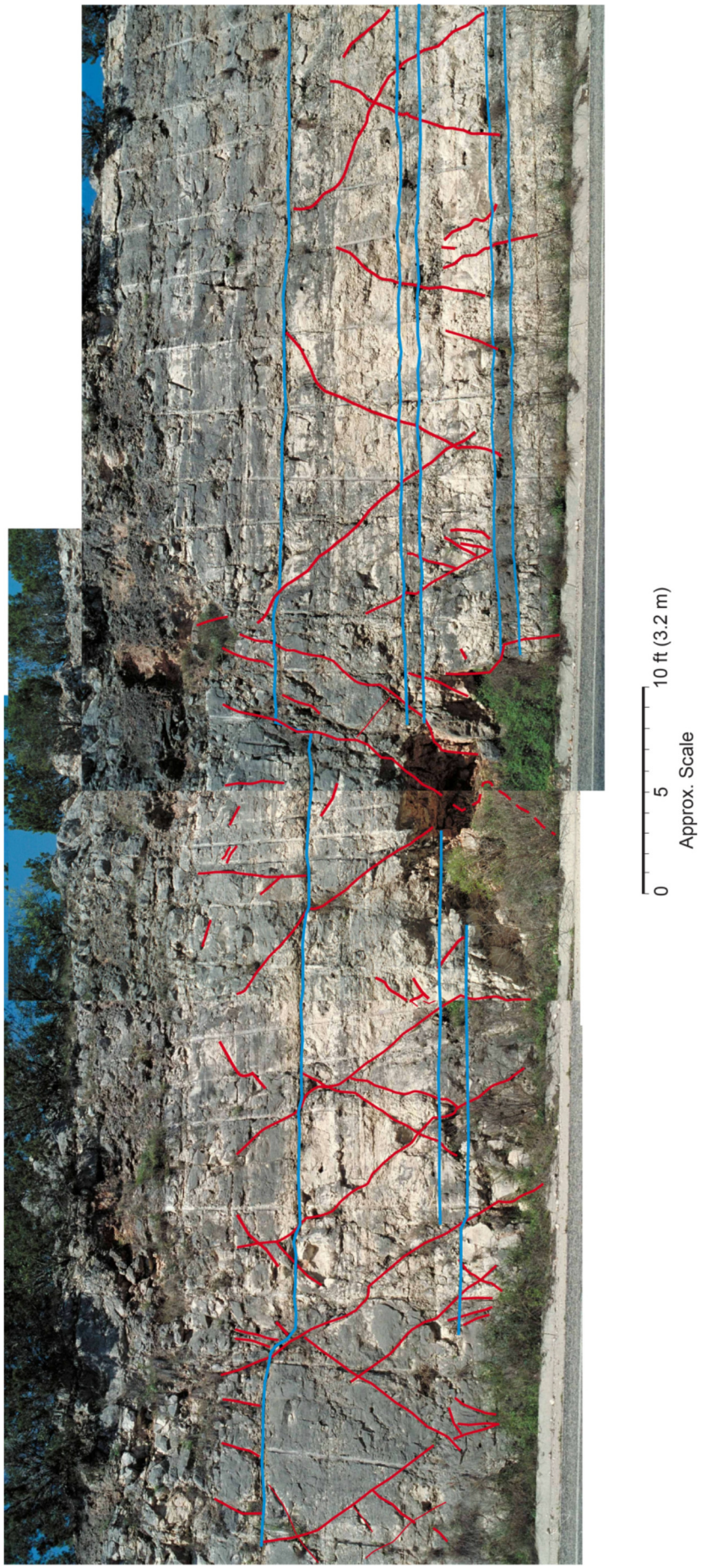

Figure 7. West face of road cut showing two small caves and a graben. Major fractures are marked in red. Beds 2 and 4 as well as the upper marly bed are marked in blue. Photo is oriented north (right) and south (left).

Association of Petroleum Geologists Bulletin, v. 79, p. 1275–1300.

Veni, G., 1987, Fracture permeability: Implications on cave and sinkhole development and their environmental assessments, *in* B. F. Beck and W. L. Wilson, eds., Karst hydrogeology: Engineering and environmental applications: Proceedings of the 2nd Multidisciplinary Conference on Sinkholes and the Environmental Impacts of Karst, University of Central Florida, Florida Sinkhole Research Institute, Orlando, v. 2, p. 101–105.

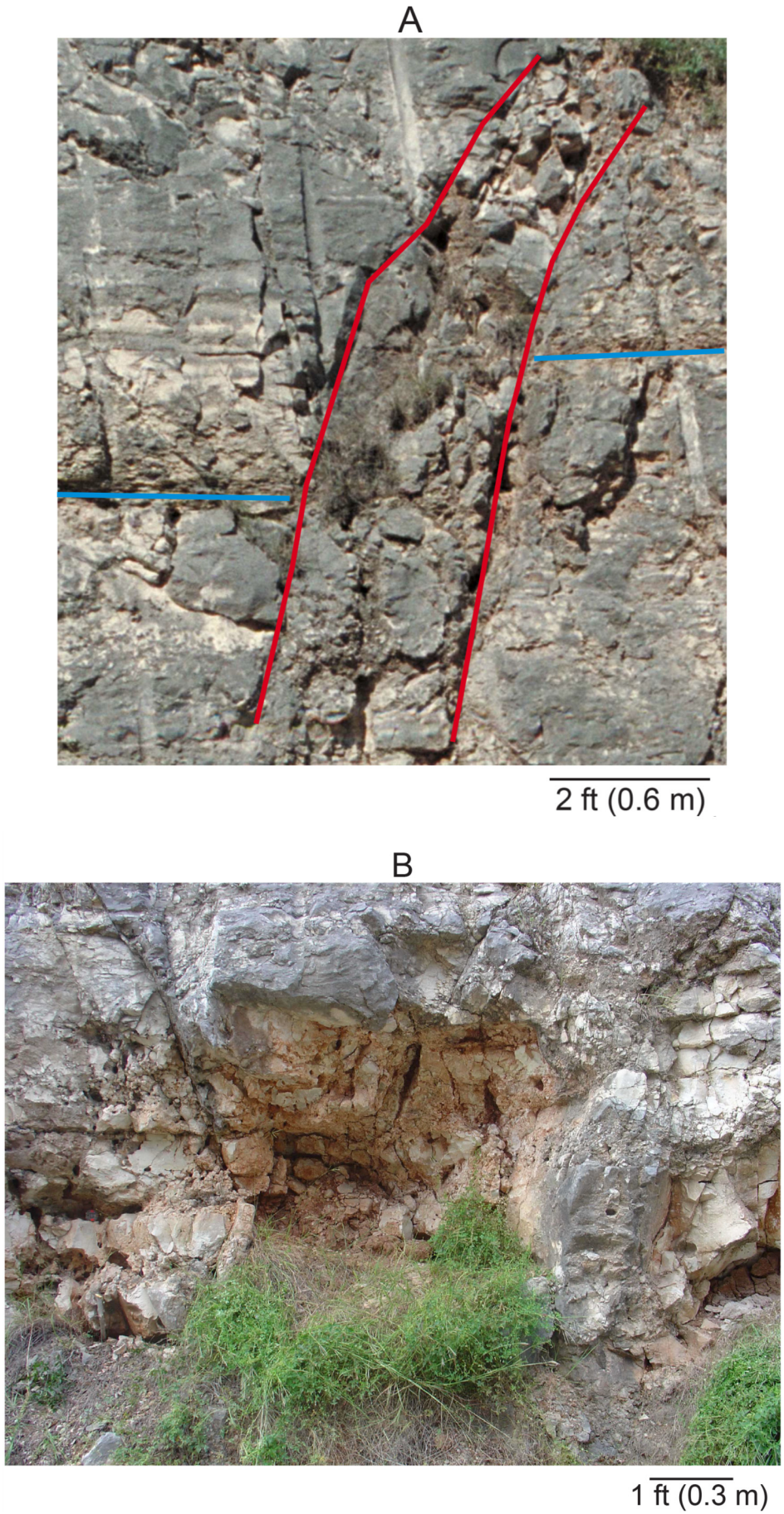

Figure 8. East side fault. (A) Fault breccia along north graben fault. (B) Small cave showing dissolution on cave walls.

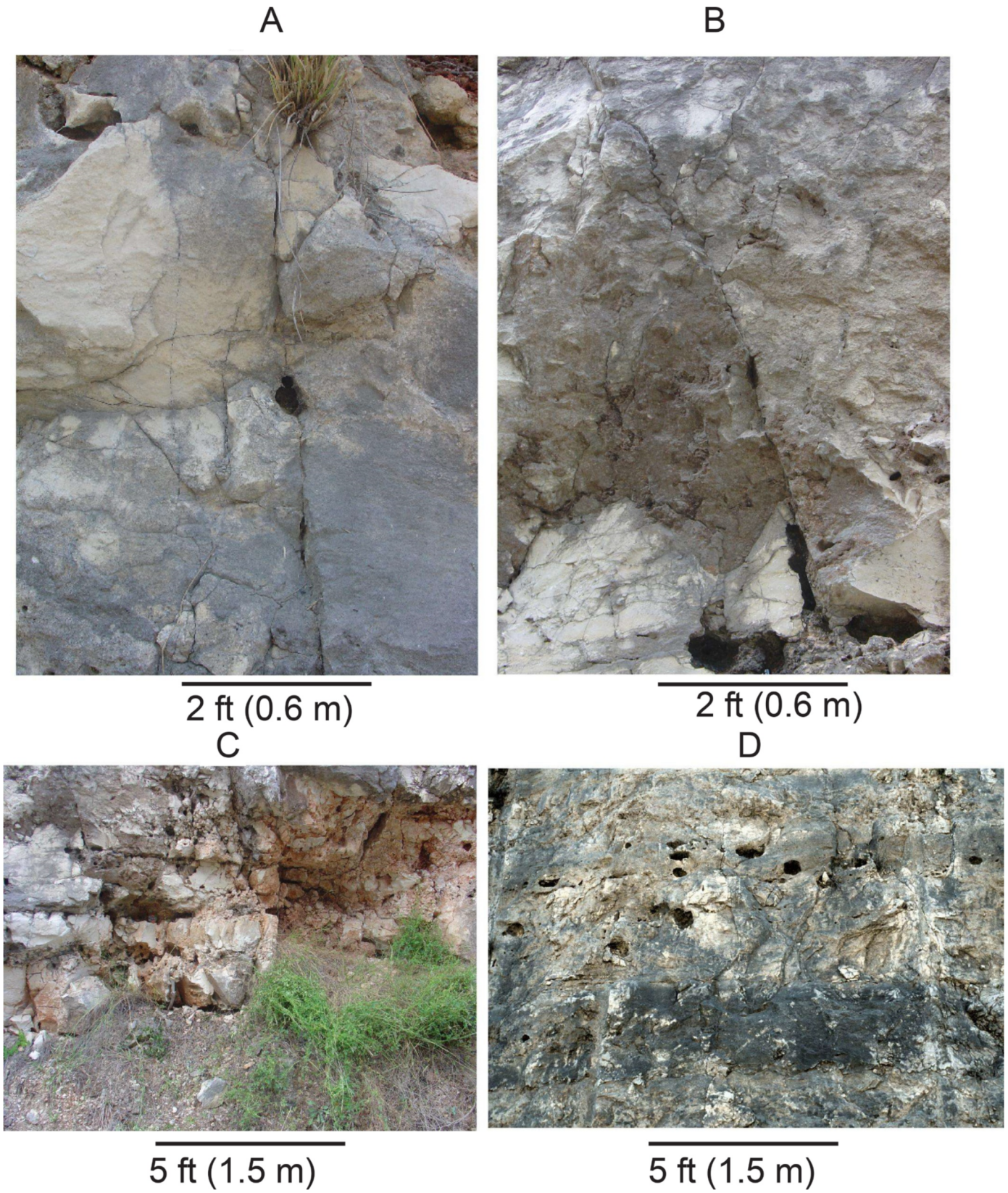

Figure 9. Examples of vugs observed. (A) Small vug along a fracture trace. (B) Solution-enlarged fracture. (C) Bedding-plane dissolution. (D) Isolated vugs that may be dissolved anhydrite nodules.

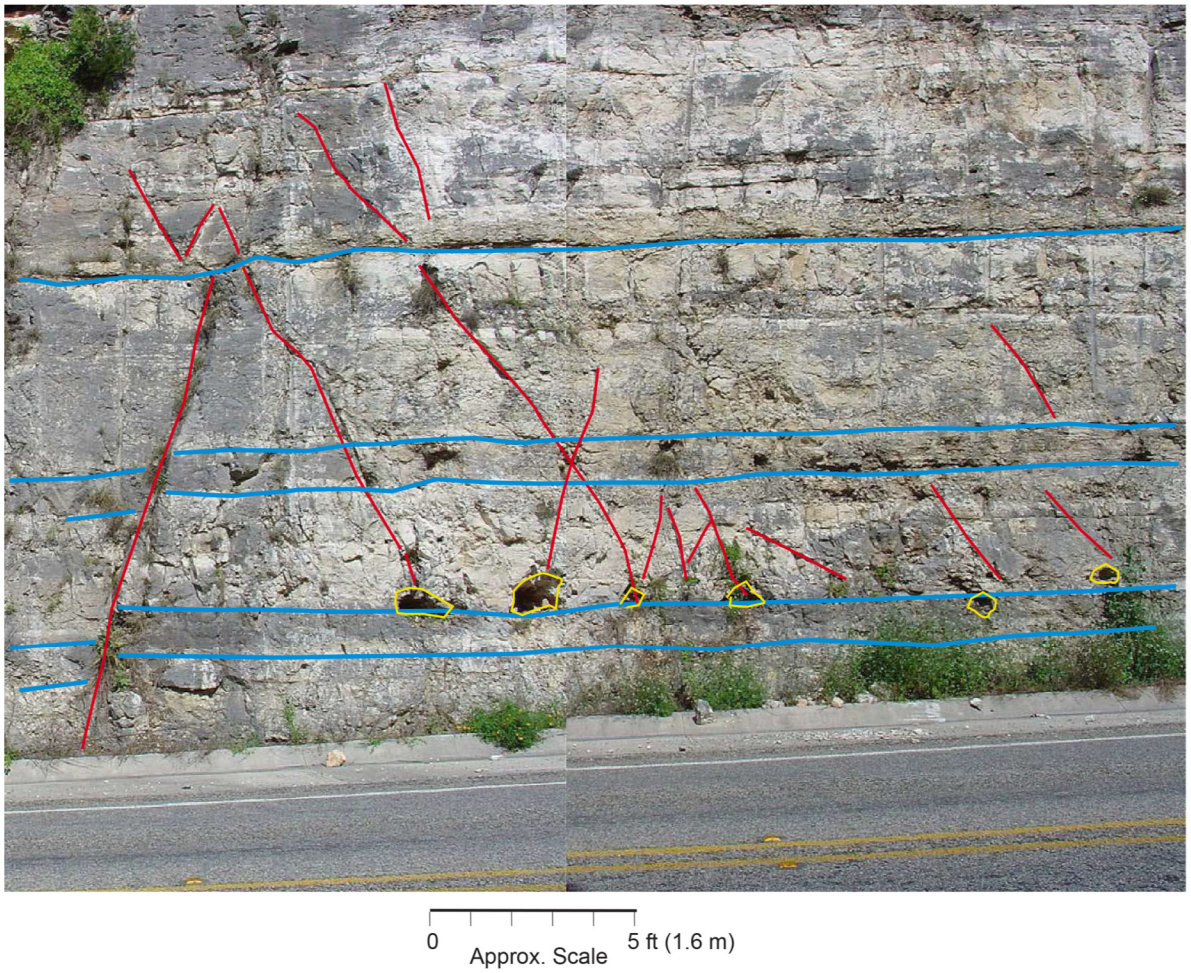

Figure 10. West face showing bedding-specific vugs (yellow) associated with fractures (red) and permeable beds 2 and 4 (blue). Upper marly bed is also shown in blue.

Figure 11. Histogram of vug sizes that have a flooring of soil.

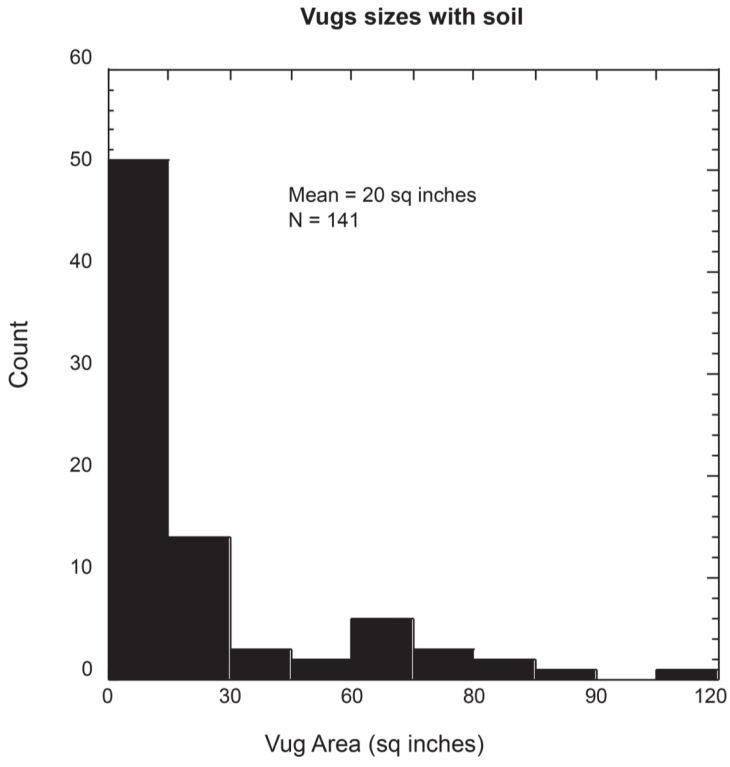

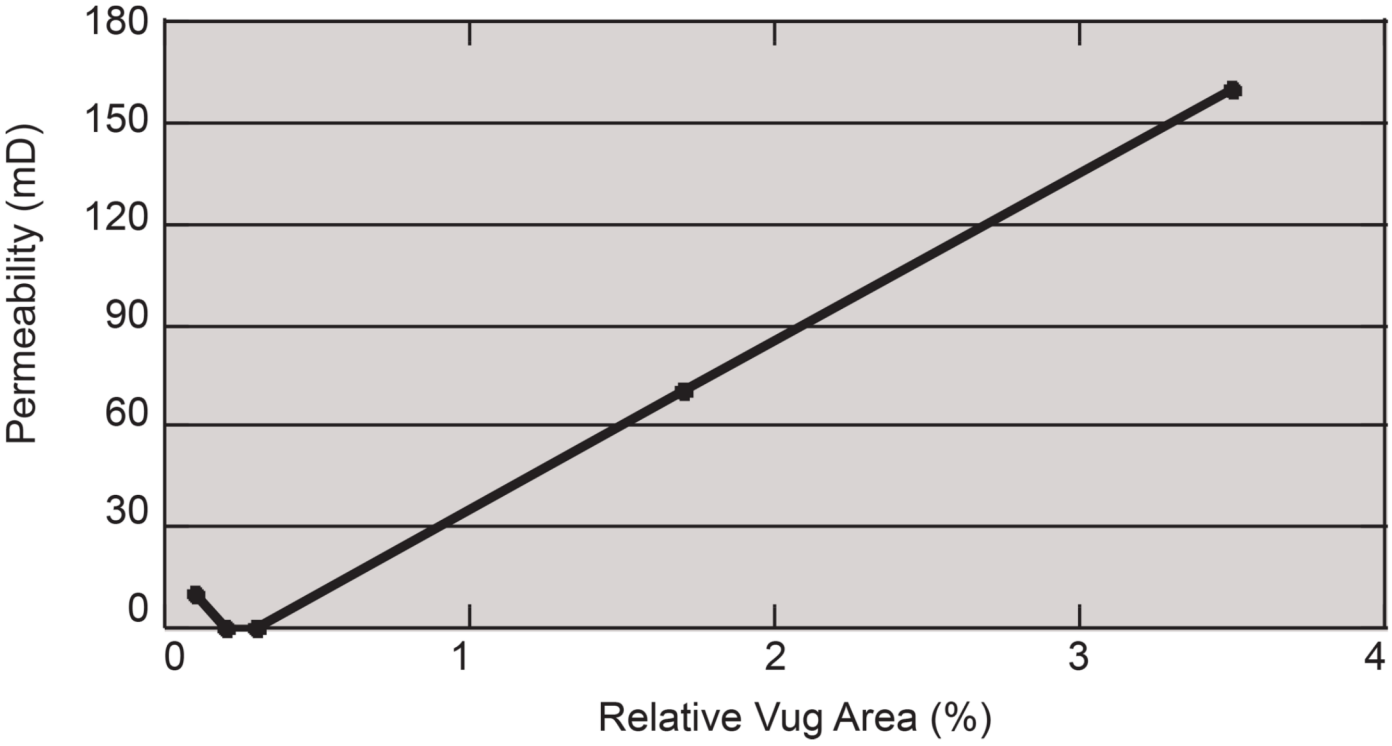

Figure 12. Correlation between relative vug area and air permeability from plugs for beds 1 through 7 less bed 6 (modified after Kurtzman et al., 2007). Only 56 vugs that contain soil are used.

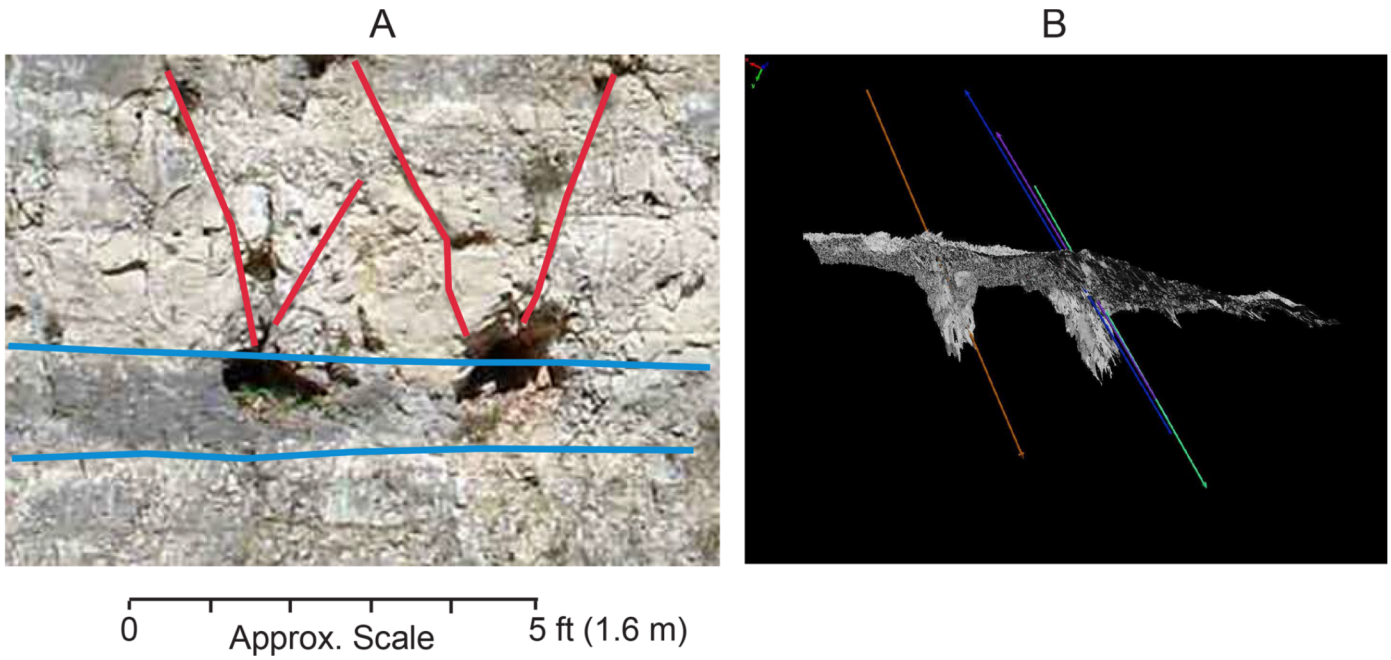

Figure 13. East wall. (A) Two large vugs in bed 2 and associated fractures. (B) Lidar image focused inside the vugs showing linear trends parallel to the strike of the fractures.

APPENDIX A

Twelve core plugs were collected from bed 2 along a 52 ft (16 m) horizontal traverse by Dr. Kurtzman. The results are displayed below (Table A–1). The permeability of the grain-dominated packstones varies by a little more than one order of magnitude, from 3 to 129 md, and averages 53 md. Porosity averages 13%.

Table A–1. Description of horizontal core plugs in bed 2. Plus signs indicate sense of relative abundance.

Distance	Lithology	Rock Fabric	Visible pore space			Porosity	Perm.
ft (m)			Interpartical Porosity	Separate-Vug Porosity	Touching-Vug Porosity	%	md
13.5 (4.1)	Limestone	Wackestone	no	no	Fracture	3.5	4.53
20.0 (6.1)	Limestone	Grain-Dominated Packstone	yes	moldic++		20.1	112.08
23.3 (7.1)	Limestone	Grain-Dominated Packstone	yes	moldic+++		16.3	48.10
26.7 (8.1)	Limestone	Wackestone	no	no		5.2	0.56
29.9 (9.1)	Limestone	Wackestone	no	no		4.1	0.19
33.1 (10.1)	Limestone	Grain-Dominated Packstone	yes	moldic+		9.2	6.28
39.7 (12.1)	Limestone	Grain-Dominated Packstone	yes	moldic++		15.2	62.12
43.0 (13.1)	Limestone	Grain-Dominated Packstone	yes	moldic++		10.4	26.15
49.5 (15.1)	Limestone	Grain-Dominated Packstone	yes	moldic+		9.1	3.02
52.8 (16.1)	Limestone	Grain-Dominated Packstone	yes	moldic+		12.9	88.42
62.7 (19.1)	Limestone	Grain-Dominated Packstone	yes	moldic++		17.3	129.50
65.9 (20.1)	Limestone	Grain-Dominated Packstone	yes	moldic++		11.4	9.01